THE AMERICAN SOCIETY OF MECHANICAL ENGINEERS
345 E. 47 St., New York, N.Y. 10017

The Effects of Friction in Axial Splines on Rotor System Stability

ANTONIO F. ARTILES
Mechanical Technology Inc.
Latham, New York 12110

ABSTRACT

An in depth parametric evaluation of the effects of Coulomb friction in an axial spline joint on the stability of the rotor-bearing system was conducted through time transient integration of the equations of motion. Effects of: spin speed, friction coefficient, spline torque, external damping, imbalance and side load as well as asymmetric bearing stiffnesses were investigated.

A subsynchronous instability is present at the bending critical speed when the spin speed is above this critical. The limit cycle orbit is circular, is proportional to the product of the friction coefficient and spline torque (μT), is inversely proportional to the external damping and is independent of spin speed.

When imbalance is applied to the rotor, beating between the subsynchronous natural frequency and the synchronous (spin speed) frequency occurs. The subsynchronous component of the orbit is proportional to μT, while the synchronous component is proportional to the imbalance.

When a static side load is applied, the unstable node at the center of the orbitally-stable limit cycle grows into an elliptical orbitally-unstable limit cycle, separating stable - from unstable regions of the phase plane. Below a threshold value of side load, the transient motion approaches one of two asymptotic solutions depending on the initial conditions: the larger stable limit cycle or a point at the center of the smaller unstable limit cycle. Beyond the threshold value of side load the rotor-bearing system is stable and all motions decay to a point.

Asymmetry in the bearing stiffnesses reduces the size of the subsynchronous whirl orbit.

1.0 INTRODUCTION

Stability of rotor-bearing systems has been studied by numerous authors, such as Gunter [1], Black [2], Glasgow [3] and more recently, Lund [4]. Internal rotor friction has been demonstrated [5], both analytically and experimentally, to cause instability in rotors operating above their first bending critical. Turbopumps such as the Space Shuttle Main Engine (SSME) High Pressure Oxidizer Turbopump (HPOTP) contain friction joints such as interference fits and splines. These rotors may operate above flexible bending criticals and have relatively light external damping, both of which are potential conditions for instability.

This paper is concerned with the evaluation of the effects of the system parameters on the stability of a rotor that contains two spline joints. The parameters investigated were: spin speed, friction coefficient, spline torque, external damping, imbalance, side load and asymmetry in bearing stiffnesses.

2.0 ROTOR MODEL, NUMERICAL APPROACH AND INITIAL CONDITIONS

Figure 1 shows the rotor-bearing model used to exercise the spline. It consists of a shaft mounted on ball bearings at the ends with a spline sleeve in the middle. Spline couplings at the ends of the sleeve connect it to the rotor. External damping to ground is applied at the sleeve. The spline configuration is the same as that in the SSME HPOTP rotor. This same spline was tested in a rotor-dynamic test rig, similar to the model in Figure 1, which showed a very strong subsynchronous whirl at the first critical, as reported in [1]. The first undamped natural frequency of the system corresponds to a bending critical at 1247 RPM. Figure 2 is a plot of the corresponding mode shape, showing the relatively large bending of the shaft at the sleeve ends and the relatively small deflection at the bearings.

NOMENCLATURE

$\Delta\theta$, $\Delta\alpha$	difference in angular displacements across the spline measured in coordinate systems fixed on the ground and fixed on the rotor, respectively.
K_a	angular stiffness of the spline.
T	steady torque transmitted by spline.
U_f, U_v	energy contributions per cycle due to spline friction and external damper, respectively.
μ	coefficient of friction.
Ψ	spline teeth pressure angle.
Ω	spin speed of rotor.

Presented at the International Gas Turbine and Aeroengine Congress and Exposition
Orlando, FL June 3-6, 1991
This paper has been accepted for publication in the Transactions of the ASME
Discussion of it will be accepted at ASME Headquarters until September 30, 1991

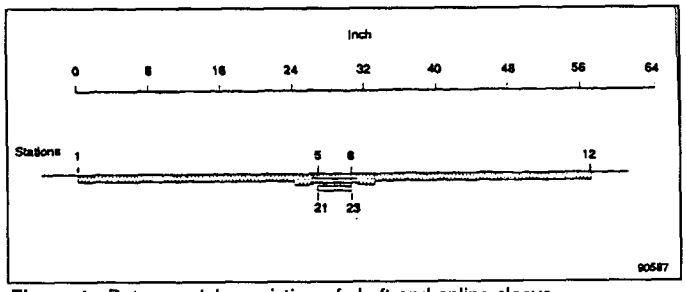

Figure 1. Rotor model consisting of shaft and spline sleeve.

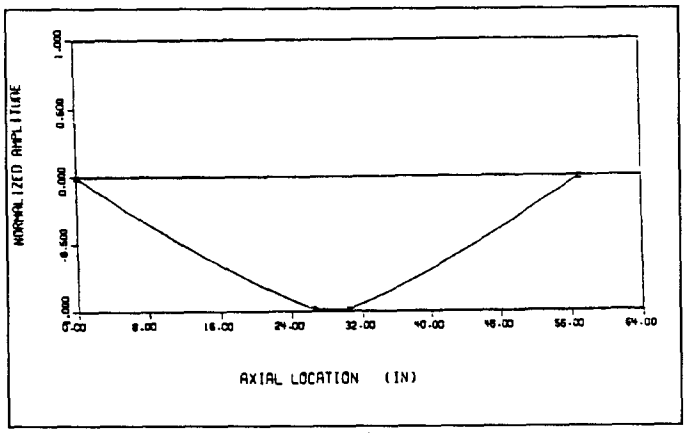

Figure 2. Mode shape for first natural frequency

A Coulomb friction model that describes analytically the behavior of a spline coupling was developed in [1], showing that the moment transmitted across the spline joint is given by:

$$-\boldsymbol{M} = K_a \Delta\boldsymbol{\theta} + \frac{2\mu T}{\pi \cos\Psi} \frac{\Delta\dot{\boldsymbol{\alpha}}}{|\Delta\dot{\boldsymbol{\alpha}}|} \tag{1}$$

$$\boldsymbol{M} = \begin{Bmatrix} M_x \\ M_y \end{Bmatrix} \quad \Delta\boldsymbol{\theta} = \begin{Bmatrix} \Delta\theta \\ \Delta\phi \end{Bmatrix} \quad \Delta\dot{\boldsymbol{\alpha}} = \begin{Bmatrix} \Delta\dot{\theta} + \Omega\Delta\phi \\ \Delta\dot{\phi} - \Omega\Delta\theta \end{Bmatrix}$$

where: $\Delta\boldsymbol{\theta}$ and $\Delta\boldsymbol{\alpha}$ are the differences in angular displacements across the spline measured in coordinate systems fixed on the ground and on the rotor, respectively. K_a is the angular stiffness of the spline, T is the spline torque, μ is the coefficient of friction and Ψ is the pressure angle.

When conditions are such that the relative angular velocity across the spline joint approaches zero, the joint will stick. However, the spline model is assumed to be slipping. The phenomenon of the transition from a slipping to a sticking interface was not found to be relevant to the stability question. The equations of motion were integrated versus time using a fourth-order Runge-Kutta method. The time step was made small enough to avoid numerical instability and assure accuracy of solution.

Different initial conditions were used to start the rotor transient motion. Either an imbalance force or a static side force of 1780 N [400 lbs] was applied to the rotor at rest, for 1 second and then released. Figure 3 shows the transient response orbits for these two initial conditions. In both cases, the rotor motion approaches the same circular orbit from the outside. Another simulation where the displacements and velocities after the imbalance was removed were scaled down by a factor of 0.6 is shown in Figure 4. In this case, the rotor motion approaches the same circular orbit from the inside.The parametric study is mostly concerned with the final motion of the system and not the intermediate transient. The set of displacements and velocities corresponding to the above circular limit cycle orbit was found to be the most appropriate choice of initial conditions. However,

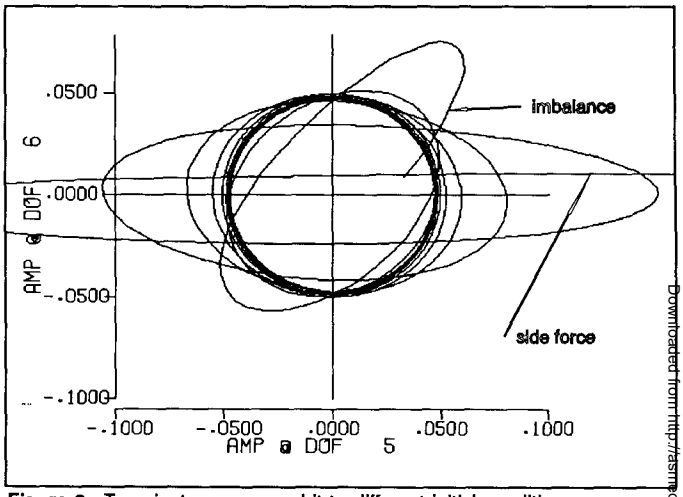

Figure 3. Transient response orbit to different initial conditions.

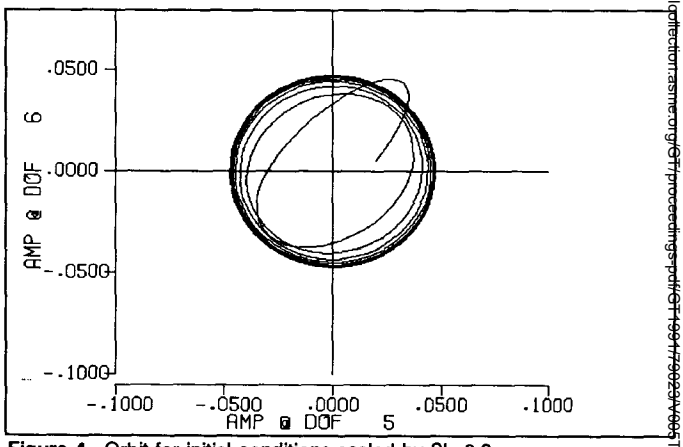

Figure 4. Orbit for initial conditions scaled by SI=0.6.

since under non-symmetric operation there were two different solutions to the final motion, a scale factor (SI) was used in order to scale the set of displacements and velocities used for initial conditions.

3.0 PARAMETRIC STUDY

3.1 Symmetric conditions.

Under symmetric conditions (no side force and isotropic bearing coefficients), when the rotor is spinning at frequency Ω and is whirling in a circular motion at frequency ω, the energy added in one cycle to the rotor-bearing system by the spline joint can be calculated to be:

$$U_f = sgn(\omega - \Omega) \frac{4\mu T r_1}{\cos\Psi} \tag{2}$$

where r_1 is the amplitude of the relative angular displacement across the joint. On the other hand, the energy contribution from a viscous damper is given by:

$$U_v = -2\pi\omega B r_2^2 \tag{3}$$

where r_2 is the radius of the circular whirl orbit at the damper location. The negative sign indicates that energy is being dissipated.

When the motion reaches its limit cycle, the net energy added to the system is zero. Setting the sum of the above two equations to zero yields the amplitude of the motion:

$$r_1 = \begin{cases} 0, \text{ if } \Omega<\omega \\ \dfrac{2\mu T}{\pi \omega B \cos\psi}\left(\dfrac{r_1}{r_2}\right)^2, \text{ if } \Omega>\omega. \end{cases} \quad (4)$$

where the ratio (r_1/r_2) is obtained from the mode shape of the motion. Below the first bending natural frequency, both energy contributions are negative, resulting in zero motion. Above the first bending natural frequency, the radius of the limit cycle orbit is proportional to the product of the friction coefficient and the spline torque (μT) and inversely proportional to the external viscous damping (B). Of course, when the rotor motion is such that the moment acting through the spline joint does not exceed that required to overcome slip ($2\mu T/\pi\cos\psi$): the joint connection will be elastic and the rotor will be stable without subsynchronous motion, in spite of operation above the first bending critical.

3.2 Imbalance

Figure 5 is a plot of three different limit cycle orbits showing the combined effects of friction and imbalance: 1)an imbalance of 890 N [200 lbs] and zero friction, 2)an imbalance of 890 N and μT=56.5 N-m [500 lb-in], and 3)zero imbalance and μT=56.5 N-m. The case with imbalance only has purely synchronous motion while the case with only friction has motion purely at the first natural frequency. For both of these cases the orbit is circular.

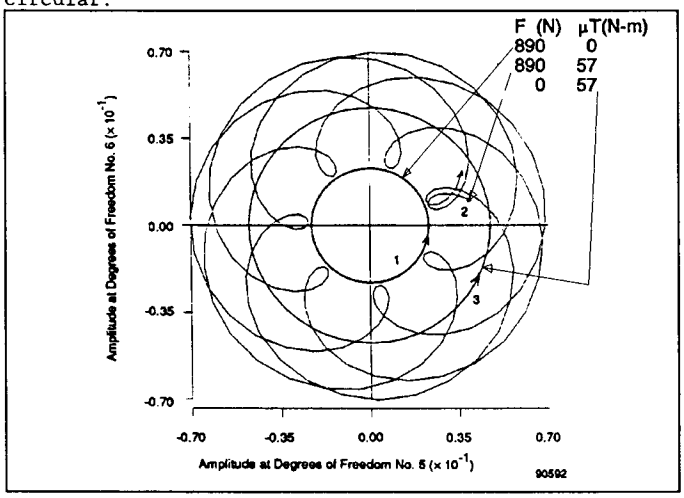

Figure 5. Limit Cycle Orbits for Different Combinations of Imbalance and Friction Torque Product.

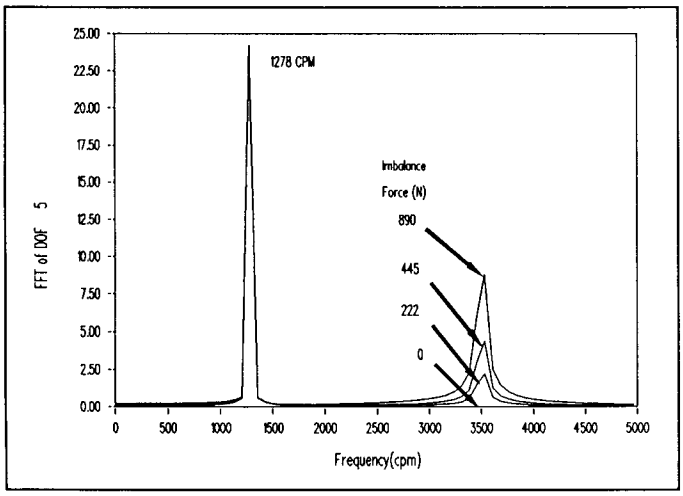

Figure 6. FFT of Lateral Motion for Different Amounts of Imbalance.

The case with both imbalance and friction shows a combined motion beating between the two frequencies and contained within an annular region. Figure 6 shows the FFT of the lateral displacement as the imbalance force is increased from zero to 890 N. Clearly, the synchronous component of motion increases in proportion to the imbalance force while the subsynchronous component is unaffected. Thus, there are two components of motion, uncoupled from each other, at two frequencies:

1. a subsynchronous component (at the first bending critical), proportional to μT/B. This component is responsible for the mean radius of the annular region.

2. a synchronous component (at the spin speed), proportional to the imbalance force. This component is responsible for the width of the annular region.

3.3 Side Load

A static side load applied to the rotor will cause a moment to be transmitted through the spline connections between the sleeve and the rotor. There exists a threshold for this side load beyond which the rotor-bearing system is stable and all motions decay to a point. Below the threshold, the transient motion will approach one of two solutions as $t\to\infty$, depending on the initial conditions, as discussed below.

In the theory of the stability of nonlinear systems, a limit cycle is defined as an isolated closed phase path[1] which corresponds to a periodic mode of operation in the system. If all neighboring phase paths approach this cycle, from both the inside and outside, asymptotically as $t\to\infty$, it is called a stable limit cycle. On the other hand, if there exists at least one neighboring phase path that does not approach this cycle as $t\to\infty$, it is called an unstable limit cycle. Similarly, a stable or unstable node is a singular point towards which or away from which all neighboring phase paths move as $t\to\infty$. For more information on this subject, see [6].

When the rotor is operating above the first bending critical and at zero side load there is an orbitally-stable circular limit cycle for the motion at a whirl frequency equal to the first bending critical, regardless of the initial conditions. The center of this circle is an unstable node.

As the side load is applied, the center of the orbitally-stable limit cycle moves in the direction of the load. This unstable node grows into an orbitally-unstable limit cycle. Figure 7 is a comparative plot of the two limit cycles as the side load is progressively increased from zero to 1780 N. The arrows indicate the stability status of the different cycles and nodes. The unstable limit cycle is elliptical in shape and has its major axis inclined a few degrees from the direction of the applied load, as can be determined by looking in more detail at the case of 890 N side load at different initial conditions. Figure 8 shows part of the orbit of the rotor near this cycle for three values of initial conditions (SI=3.5, 3.875 and 4.25) between t=0.55 and t=0.60 seconds. Figure 9 shows the complete orbits (from t=0 to 1 sec) for these three conditions. As seen, the orbit decays to a point for SI=3.5, where as it grows to the stable limit cycle for SI=4.25. For SI=3.875 on the other hand, the orbit does not depart drastically from the cycle in Figure 8 even after time has reached a full second. The criteria which determines the final orbit is not simply whether the initial rotor displacement is inside or outside this unstable limit cycle but it is a complex function of all of the initial displacements and velocities of the system.

Thus, the unstable limit cycle represents a threshold for the initial conditions of the rotor-bearing system to

[1] "Phase path" is the term given to the path of a representative point in the phase plane, while "phase" is used to describe the state of the system, i.e., the set of displacements and velocities of the system at a given time.

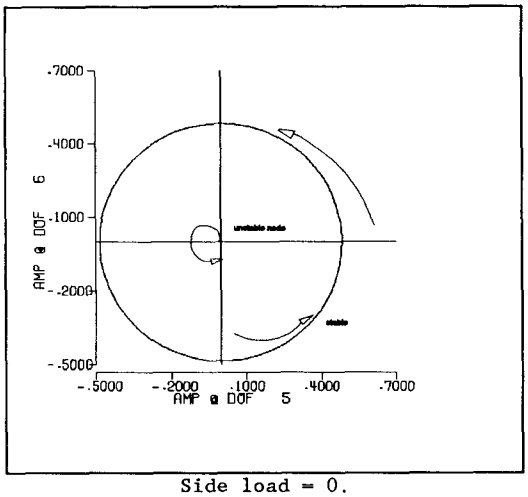

Side load = 0.

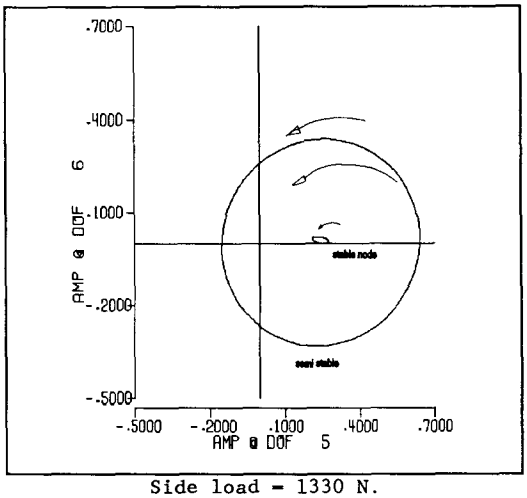

Side load = 1330 N.

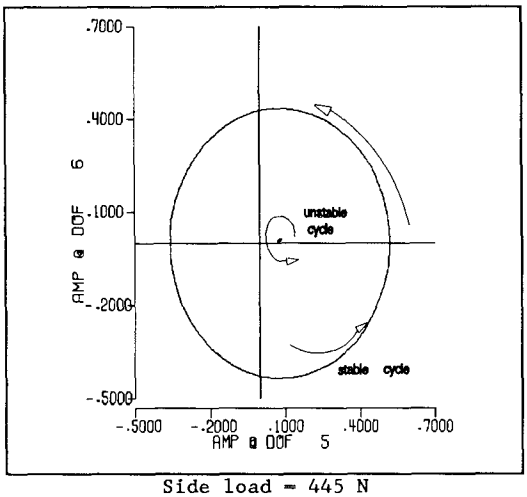

Side load = 445 N

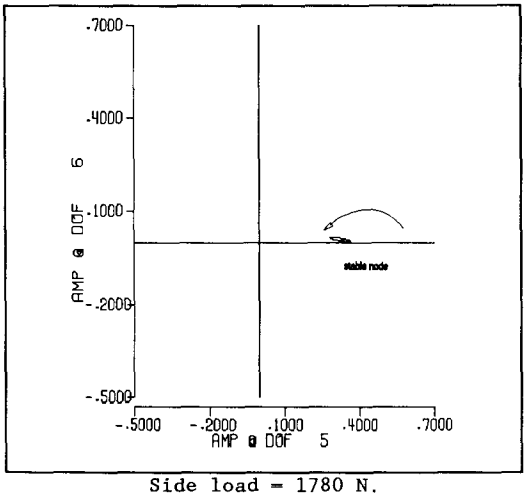

Side load = 1780 N.

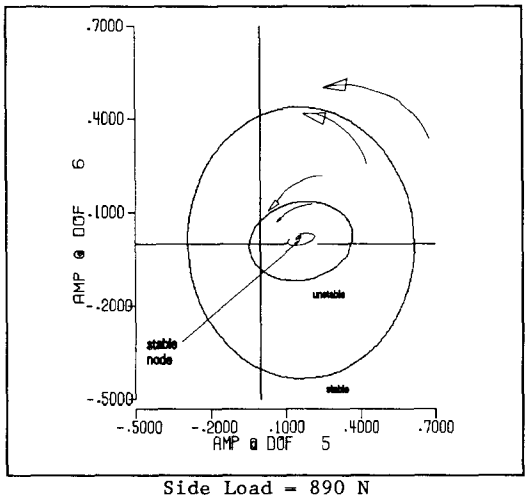

Side Load = 890 N

Figure 7. Comparison of orbitally stable (Larger) and orbitally unstable (smaller) limit cycles at different side loads.

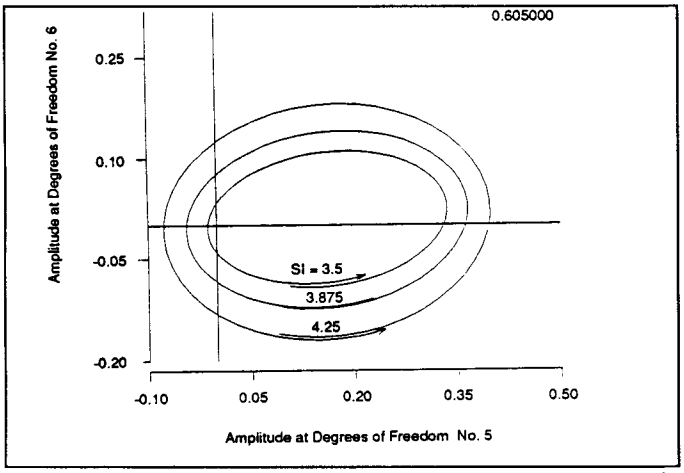

Figure 8. Transient orbit for three different initial conditions near the unstable limit cycle between t= 0.55 and 0.65 sec.

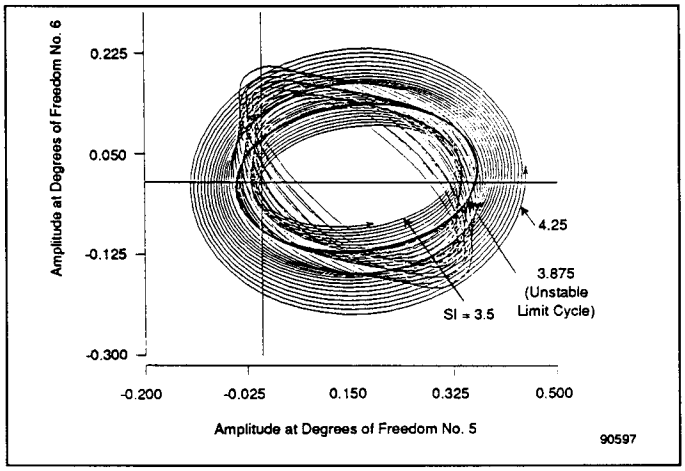

Figure 9. Transient orbit for three different initial conditions near the unstable limit cycle between t= 0 and 1 sec.

eventually reach the non-zero orbitally-stable limit cycle, which is manifested as a subsynchronous vibration. For small initial conditions, the transient orbit will decay in an elliptically-shaped spiral towards a point at its center which is now a stable node. Figure 10 illustrates the transient orbits for three different values of small initial conditions (SI= 3.5, 2 and 1). On the other hand, for large enough initial conditions, the orbit grows towards the larger, more-circular stable limit cycle, from either the inside or the outside. Figure 11 illustrates the transient orbits for three different values of large initial conditions (SI= 5, 10 and 20).

As the side load is increased, the orbitally-unstable limit cycle grows very rapidly towards the larger limit cycle. This larger cycle, on the other hand, decreases and becomes elliptical very gradually with increasing side load. The principal axis of this larger cycle is along the direction of load. Both limit cycles merge into one another at the threshold of side load (about 1330 N for this case) to form what is called a "semi-stable" or double cycle[2]. Although motions with large initial conditions approach this cycle asymptotically from the outside, any disturbance will cause the motion to decay towards the stable node at its center.

Figure 12 contains superimposed plots of the envelopes of the lateral component of motion versus time for numerous values of the initial condition scale factor (SI) and a side load of 100 lbs. Figures 13, 14 and 15 are similar plots for side loads of 890, 1330 and 1780 N,

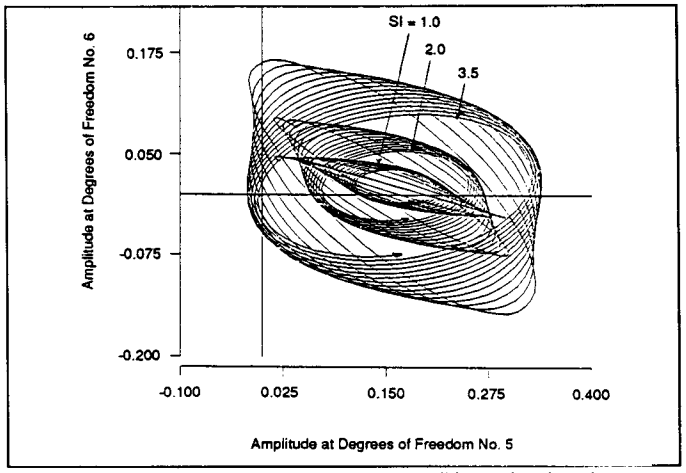

Figure 10. Transient orbit for small initial conditions showing decay to a stable node.

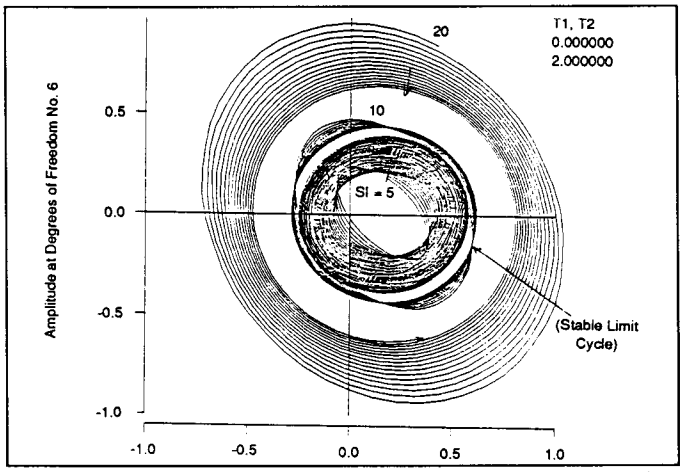

Figure 11. Transient orbit for large initial conditions showing approach to stable limit cycle.

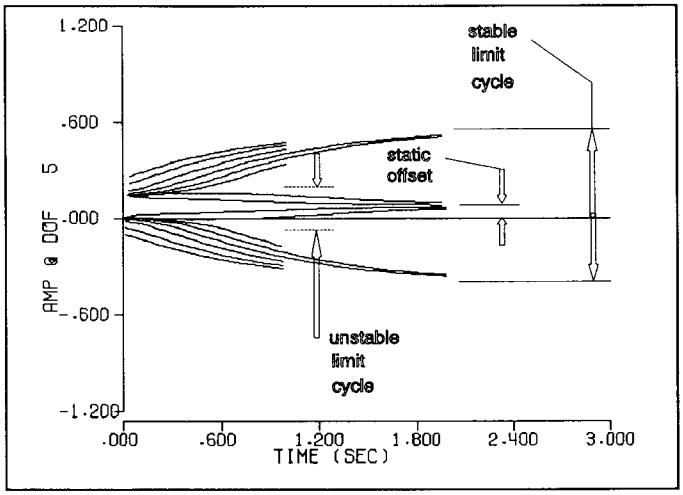

Figure 12. Envelopes of Lateral Motion versus time for different initial conditions at 445 N side load.

respectively, except for a factor of 2 in the scale of the abscissa. At large orbit amplitudes (near the limit cycles) the decay rate with time is fairly slow while as the orbit size decreases the decay rate rapidly

increases. Further increase in side load beyond the threshold increase the rate of decay of the motion towards the stable node at the static offset. This is shown in the plots of the envelops for the case of a side load of 1780 N (Figure 15) which do not show any evidence of a limit cycle.

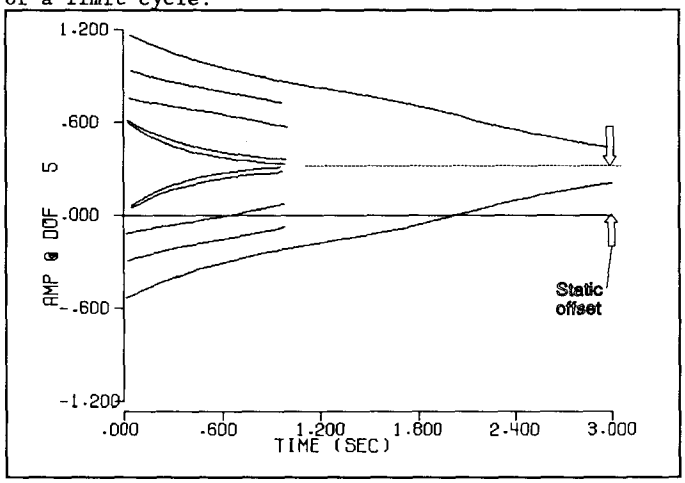

Figure 13. Envelopes of lateral motion versus time for different initial conditions at 1780 N side load.

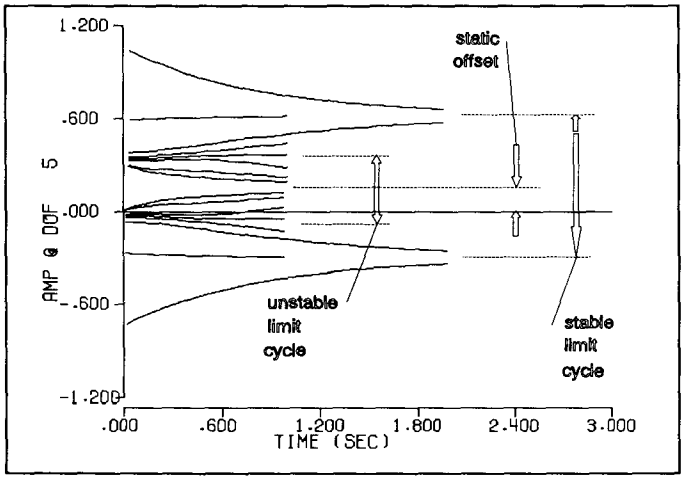

Figure 14. Envelopes of lateral motion versus time for different initial conditions at 890 N side load.

Figure 16 plots the size and ellipticity of the stable limit-cycle orbit as the side load is increased. The orbit starts out as a large circle which becomes elliptical and shrinks in size, very slowly for small side load and then very rapidly as the threshold (1780 N) is approached.

3.4 Asymmetric bearing coefficients

Figure 17 shows the effect of decreasing one of the components of direct bearing stiffness (K_{yy}) on the limit cycle orbit. As K_{yy} is decreased from 100,000 to 10,000 lb/in, the orbit becomes elliptical with the major axis inclined about 135° from the x-axis and increasing to about 110% of the radius of the original circular orbit. Further decrease in K_{yy} decrease the size of the orbit without much further effect on its ellipticity. Figure 17 is a plot of the major and minor axes of the limit cycle ellipse. In the case of this rotor model, no reduction in the major axis is noticed until K_{yy}/K_{xx} is less than 10%. However, as shown by the mode shape in Figure 2, the rotor model utilized here to exercise the joint is fairly flexible compared to the bearing stiffness. A stiffer rotor would involve more participation of the bearings in the first bending mode. Therefore, it is expected that for relatively stiffer

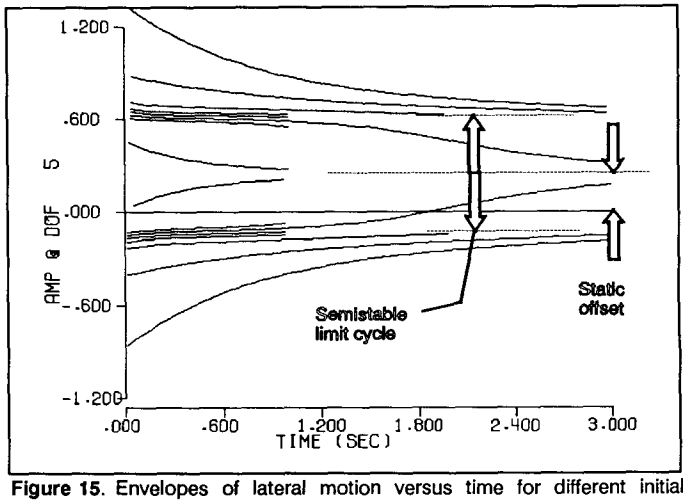

Figure 15. Envelopes of lateral motion versus time for different initial conditions at 1330 N side load.

rotors, asymmetry in the bearing coefficients should have a more beneficial effect in controlling rotor instability.

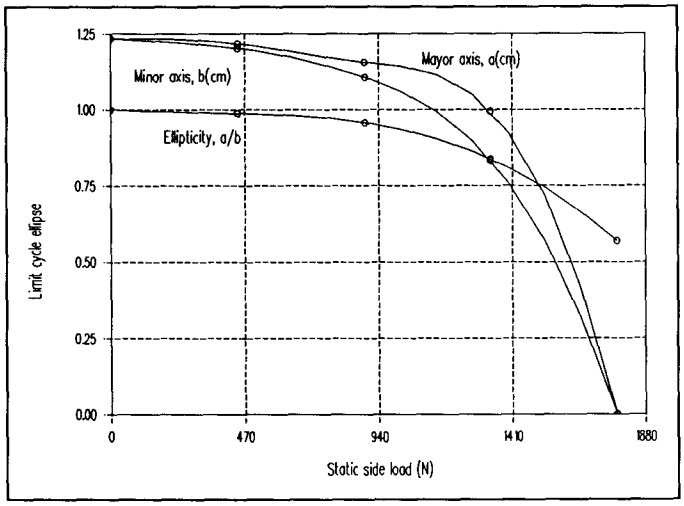

Figure 16 . Effect of side load on limit cycle.

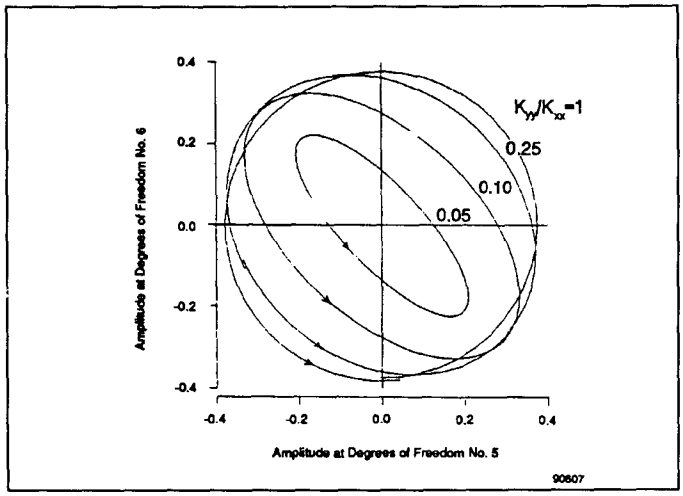

Figure 17. Limit cycle orbits versus increasing bearing stiffness asymmetry.

3.5 Rotating Speed

The rotor will be stable or unstable depending on whether the rotating speed is lower or higher than the first bending critical speed of the rotor-bearing system. Several simulations performed with and without side load showed no effect of speed. Other than determining the stability status, the spin speed has no noticeable effect on the size of the orbit or on the transient motion to reach it. (The only effect is through the small influence that the gyroscopic effects have on the first bending critical speed and mode shape.)

4.0 CONCLUSIONS

For symmetric operation:

1. There is only one asymptotic solution (as $t \to \infty$) independent of the initial conditions. If the spin speed is less than the first bending critical speed, the energy contribution from the friction in the spline is negative, resulting in zero subsynchronous motion and a stable rotor. If the spin speed is greater than the first bending critical speed, the rotor is unstable and its motion is a circular limit cycle whirling at a frequency equal to the first rotor bending critical. The radius of this limit cycle orbit is proportional to the product of the friction coefficient and the spline torque, and is inversely proportional to the external viscous damping. Transient motions proceed in spiral paths, from either the inside or the outside, towards the limit cycle circle. The center of the circle is an unstable node.

2. Other than determining whether instability is present or not, there is very little effect of spin speed on the size of the subsynchronous motion, only the small influence that the gyroscopic effects have on the first bending critical speed and mode shape.

3. With rotor imbalance the limits of the rotor orbit widen from a circle to an annulus. The motion within this annulus contains two components at two frequencies: a subsynchronous component (at the first bending critical) and the synchronous component. The subsynchronous component is proportional to the product of the friction coefficient and the spline torque. The synchronous component is proportional to the imbalance force and is responsible for the width of the annular region. Both components are uncoupled from each other.

Bearing asymmetry:

4. Asymmetry in rotor bearing stiffness coefficients reduces the size of the subsynchronous whirl orbit brought about by internal friction.

Static side load:

5. There exists a threshold for the side load beyond which the rotor-bearing system is stable and all motions decay to a point. Below the threshold, the transient motion will approach one of two asymptotic solutions depending on the initial conditions.

6. As the side load is applied, the unstable node at the center of the orbitally-stable limit cycle moves in the direction of the load and grows into an orbitally-unstable limit cycle. For small initial conditions, the transient orbit will decay in an elliptically-shaped spiral towards a point at its center which is now a stable node. On the other hand, for large enough initial conditions, the orbit grows towards the larger, more-circular stable limit cycle, from either the inside or the outside. As the side load is increased, the orbitally-unstable limit cycle grows very rapidly towards the larger limit cycle. This larger cycle, on the other hand, decreases and becomes slightly elliptical.

7. Both limit cycles merge into one another at the threshold of side load to form a "semi-stable" or double cycle. Although motions with large initial conditions approach this cycle asymptotically from the outside, any disturbance will cause the motion to decay towards the stable node at its center. Further increase in side load beyond the threshold increase the rate of decay of the motion towards the stable node at the static offset.

5.0 REFERENCES

1. Gunter, E.J., "Dynamic Stability of Rotor-Bearing Systems". NASA SP-113, Office of Technical Utilization, U.S. Government Printing Office, 1966.

2. Black, H. F., "The Stabilizing Capacity of Bearing of Flexible Rotors with Hysterisis", J. Eng. Ind., Trans. ASME, Feb. 1976, pp.87-91.

3. Glasgow, D.A., Nelson, H. D., "The Stability of Rotor-Bearing Systems Using Component Mode Synthesis", J. Mech.Des., Trans. ASME, v 102, n 2, Apr. 1980.

4. Lund, J.W., "Destabilization of Rotors from Friction in Internal Joints with Micro-slip," International Conference on Rotordynamics, JSME, Sept. 14-17, 1986.

5. Mechanical Technology Incorporated, "Internal Rotor Friction Instability," Technical Report 88TR39, Prepared for NASA Marshall Space Flight Center, under contract No. NAS8-35601, February 1990.

6. Andronov, A.A., Vitt, A.A., and Khaikin, S.E., "Theory of Oscillators," Dover Publications, N.Y. (1966), pg. 289.